# A HYBRID QUANTUM-CLASSICAL FUSION NEURAL NETWORK TO IMPROVE PROTEIN-LIGAND BINDING AFFINITY PREDICTIONS FOR DRUG DISCOVERY

*L. Domingo[1⋆], M. Chehimi[1], S. Banerjee[2], S. He Yuxun[2], S. Konakanchi[2], L. Ogunfowora[2], S. Roy[2], S. Selvarajan[2], M. Djukic[1] and C. Johnson[1⋆]*

[2] Ingenii Inc., New York, USA,

[1] Purdue University, The Data Mine, USA ,

⋆Corresponding Author' Emails: laia@ingenii.dev

## ABSTRACT

The field of drug discovery hinges on the accurate prediction of binding affinity between prospective drug molecules and target proteins, especially when such proteins directly influence disease progression. However, estimating binding affinity demands significant financial and computational resources. While state-of-the-art methodologies employ classical machine learning techniques, emerging hybrid quantum machine learning models have shown promise for enhanced performance, owing to their inherent parallelism and capacity to manage exponential increases in data dimensionality. Despite these advances, existing models encounter issues related to convergence stability and prediction accuracy. This paper introduces a novel hybrid quantum-classical deep learning model tailored for binding affinity prediction in drug discovery. Specifically, the proposed model synergistically integrates 3D and spatial graph convolutional neural networks within an optimized quantum architecture. Simulation results demonstrate a 6% improvement in prediction accuracy relative to existing classical models, as well as a significantly more stable convergence performance compared to previous classical approaches. Moreover, to deploy the proposed framework over today's *noisy intermediate-scale quantum (NISQ)* devices, a novel quantum error mitigation algorithm is proposed. This algorithm outperforms existing techniques and provides optimal error mitigation for error probabilities $p \leq 0.05$, while resulting in no additional overhead during the training and testing phases.

***Index Terms*—Quantum machine learning (QML), drug discovery, binding affinity, quantum fusion model.**

## I. INTRODUCTION

The healthcare landscape has undergone a transformative shift, notably marked by advancements in drug discovery through the integration of emerging technologies with conventional techniques. Through complex molecular interactions and precise computational modeling of compound interactions, novel drugs are rigorously designed and identified. Central to this drugs design process is the understanding of proteins and their role in disease mechanisms [1].

In the field of drug discovery, it is imperative to identify proteins that are instrumental in the cascade of molecular interactions leading to a specific disease [2]. Upon the identification of such a target protein, a list of prospective drug candidates is generated. These candidates, often described as small molecules or compounds termed *ligands*, have the potential to modulate the target protein's activity through binding interactions [3]. Ideal ligands are chosen based on their high binding affinity to the target protein, coupled with minimal off-target interactions with other proteins. However, quantifying such binding affinities is a resource-intensive endeavor [4], both in terms of time and financial investment. This is particularly true considering that the initial screening process often encompasses thousands of compounds [4], [5].

The transition from conventional laboratory methods to computer-aided design (CAD) has markedly improved the efficiency and accuracy of drug discovery and binding affinity prediction. This advancement has been further bolstered by the incorporation of artificial intelligence (AI) and machine learning (ML) algorithms, which facilitate exhaustive analyses of large-scale datasets, uncovering previously undetected patterns related to the atomic features of protein-ligand molecular complexes [6]. Furthermore, recent strides in quantum computing have added another layer of sophistication to drug discovery efforts, offering unprecedented parallelized computational capabilities [7]. Quantum machine learning (QML) models, in particular, are well-suited to manage the challenges of exponentially increasing data dimensionality, often outperforming traditional ML models under specific conditions. Taken together, these technological advancements make QML and hybrid quantum-classical models highly promising for navigating the complex, high-dimensional challenges intrinsic to drug discovery [8]. The main challenge facing such QML models is the noise prevalent in today's *noisy intermediate-scale quantum (NISQ)* computers, which requires advanced quantum error mitigation techniques to yield a scalable and accurate performance.

*Related Works:* Several prior works [9]–[13] addressed the problem of binding affinity prediction in drug discovery using tools from both classical ML and QML. For instance,

All Purdue authors contributed equally.

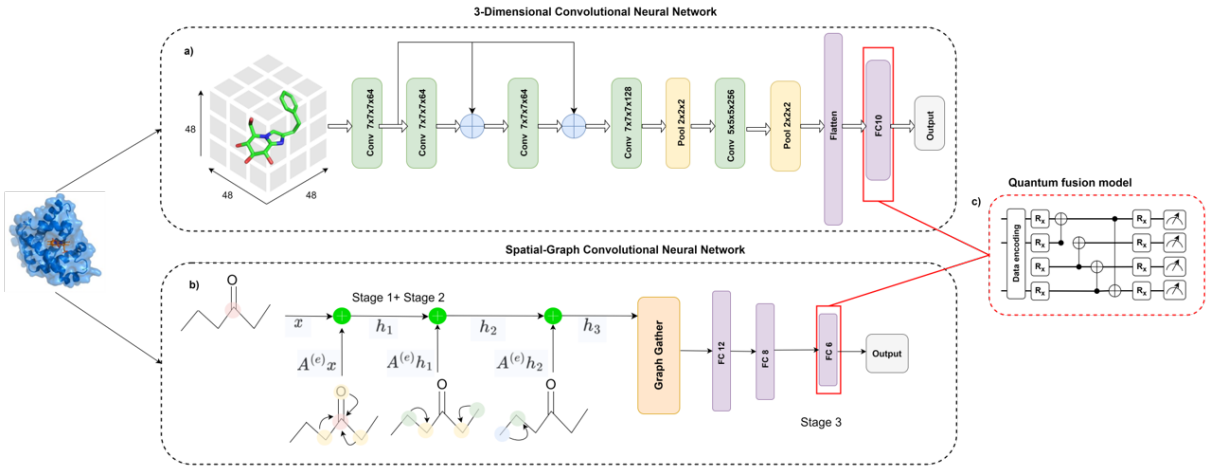


**Fig. 1**. a) 3D-CNN architecture. b) SG-CNN architecture c) Proposed hybrid quantum fusion model. In the hybrid fusion model, outputs from the second-to-last layer of each of the 2 classical neural networks trained with the PDBbind dataset are encoded onto quantum states before being fed into a feed-forward quantum neural network (QNN).

the work in [9] leveraged 3D-convolutional neural networks (3D-CNNs) to perform protein-ligand binding affinity predictions in a faster and more efficient manner relative to other ML models. Moreover, the work in [10] enhanced the model proposed in [9] by predicting binding affinities using an ensemble of several independently-trained 3D-CNN network layers. Furthermore, the work in [11] introduced a classical fusion model combining a 3D-CNN and a spatial graph CNN (SG-CNN). The model in [11] enhances the binding affinity prediction accuracy by concurrently processing grid-based, context-based, and graph-based protein features. However, the models proposed in [9]–[11] do not have a stable convergence, and their predictive accuracy is not optimized.

Additionally, the work in [12] uses quantum support vector machines for virtual drug screening. Although the hybrid QML model in [12] outperforms classical counterparts, its focus on a limited subset of protein-ligand features restricts the model accuracy and scalability to larger datasets. Finally, the work in [13] proposes a hybrid QML architecture, modifying a classical CNN by replacing a classical convolutional layer with an optimized quantum circuit. While the work in [13] successfully tackles the computational complexity inherent in classical neural networks, it does not yield an improvement in binding affinity predictive accuracy, thus achieving a comparable performance to classical models. On top of that, prior works [12] and [13] did not analyze how the presence of noise in practical NISQ devices impacts the performance of the quantum solution. To the best of our knowledge, no existing research has effectively tackled the issue of binding affinity prediction in drug discovery by capitalizing on the benefits of QML while simultaneously achieving high accuracy, ensuring smooth and stable convergence, and proposing error mitigation techniques to overcome practical noise in NISQ devices.

*Contributions:* The main contribution of this paper is the development of a novel hybrid quantum fusion model aimed at enhancing the binding affinity prediction in drug discovery. The proposed model strategically integrates 3D-CNNs and SG-CNNs to leverage their respective strengths in processing diverse facets of the training data. The proposed quantum architecture is meticulously designed for optimal accuracy. Simulation results demonstrate the superior performance of the proposed hybrid quantum fusion model relative to state-of-the-art classical models. Particularly, the proposed model achieves a 6% improvement in the binding affinity prediction accuracy, and exhibits faster, smoother, and more stable convergence, thereby boosting its generalization capacity. To enhance the scalability of the proposed quantum fusion model on NISQ devices, we present a novel error mitigation technique capable of effectively alleviating noise introduced in quantum circuits for error probabilities $p \leq 0.05$. This method incurs no additional overhead during both the training and testing phases, paving the way for broader QML applications over NISQ devices.

## II. SYSTEM MODEL

This section describes the proposed hybrid quantum fusion model, its components, the data used in training the model, and the necessary pre-processing steps.

### II-A. Proposed Hybrid QML Architecture

The proposed hybrid quantum fusion architecture builds upon the classical fusion model introduced in [11] while integrating quantum neural networks (QNNs) into the model design. In particular, the protein-ligand complex data (see Section II-B) is initially fed into a 3D-CNN and an SG-CNN, simultaneously. Then, late-late fusion is performed by feeding the outputs from the second-to-last layer of each

of the two respective CNNs into a quantum fusion model, which incorporates a QNN. Let us now briefly introduce the individual components of the proposed architecture, which is shown in Fig. 1.

*II-A1. 3D-CNN*

*Contributions:* CNNs are deep learning models specifically designed for processing and analyzing high-dimensional arrays such as images, volumes, or series data. Because of their ability to automatically learn and extract features from input data, they are a cornerstone of modern computer vision applications. The adopted 3D-CNN model in this work is based on the ResNet architecture with two residual blocks [14]. After each layer, the output is passed through a batch normalization followed by a nonlinear ReLU activation function. The output from the convolutional layers is then pooled, flattened, and fed through a sequence of fully connected layers, producing the final output of the model. Fig. 1(a) shows the exact architecture of the adopted 3D-CNN.

*II-A2. SG-CNN*

*Contributions:* An SG-CNN capitalizes on the benefits of convolutional layers while leveraging the structural relationships within protein-ligand complexes. In particular, an SG-CNN effectively captures and preserves spatial information using a 2D graph representation, where each edge corresponds to a bond between atoms across all molecules. For each molecule within the complex, spatial information and associated features are initially processed through a graph gated recurrent unit (GGRU), incorporating information from its nearest neighbors. The resulting output vector subsequently enters another GGRU, accumulating information from the next nearest neighbors. This pivotal stage, known as the *graph gather step*, is followed by the data passing through a sequence of fully connected layers, ultimately yielding the final output of the SG-CNN. The exact architecture of the adopted SG-CNN is shown in Fig. 1(b).

*II-A3. Quantum Fusion Model*

*Contributions:* The quantum fusion model, shown in Fig. 1(c), takes the outputs from the second-to-last layer of the two aforementioned CNN models. In particular, this input is a vector of size 16, as it entails the output of 10 nodes from the 3D-CNN and 6 nodes from the SG-CNN. By optimally fusing these two pre-final layers, this strategy effectively aggregates the acquired knowledge during the training of the CNNs, thereby achieving superior performance. Unlike the classical fusion model in Ref. [11], which is simply a one-layer feed-forward neural network, the quantum fusion model incorporates a QNN that consists of a quantum circuit divided into two blocks. The first block is the *quantum encoding* part, which maps the input data into a quantum circuit, and the second block is a *parameterized quantum circuit (PQC)*, where quantum operations are applied to retrieve information from the encoded data. In the quantum fusion model, the considered outputs of the 3D-CNN and SG-CNN models are first embedded into quantum states through quantum encoding circuits, then run through the trainable PQC.

*Quantum Encoding Techniques:* A variety of quantum data encoding techniques have been recently developed in the literature [15]. In this work, we focus on two of the most effective encoding techniques, analyzing and comparing their performance in the context of binding affinity prediction. Future works will consider alternative dimensionality reduction techniques, like the tensor train network [16], for more general higher-dimensional data to guarantee optimal training. The two considered methods are:

1) **Amplitude encoding**, where the features are encoded in the amplitudes of the quantum state in the computational basis [17]. This scheme requires only $\lceil \log_2(n) \rceil$ qubits to encode a data sample into a quantum state, where $n$ represents the input dimension of the QNN. The depth of the embedding circuit grows as $O(poly(n))$ while the number of parameters subject to optimization scales as $O(log_2(n))$.
2) **Hybrid Angle Encoding (HAE)**, where amplitude encoding is implemented using parallel blocks of independent qubits [15]. The features are divided into $b$ blocks of size $2^m - 1$, where $m$ is the number of qubits. Accordingly, $b \times m$ qubits are required to encode the whole data sample into a quantum state using the HAE.

*PQC Architecture:* After encoding the data into quantum states (or qubits), they pass through a PQC. The design of the PQC is crucial to guarantee optimal performance of the quantum fusion model [18], [19]. The PQC consists of several quantum gates which are controlled by classically-optimized parameters. A notable challenge is to choose an effective circuit that adequately represents the solution space while minimizing circuit depth and the number of parameters. Up to this point, two robust metrics have been introduced to assess the quality of PQCs [20], as discussed next.

The first metric, termed *expressibility*, gauges the PQC's capacity to explore the Hilbert space, thereby generating a diverse array of quantum states [20]. The second metric, termed *entangling capacity*, quantifies the PQC's ability to generate entangled states [21].

In this work, we examine six distinct PQC architectures, each characterized by differing levels of expressibility, entangling capacity, and number of training parameters. The goal is to identify the most optimal architecture for our quantum fusion model. Each PQC is composed of $L$ layers of quantum gates, which are depicted in Fig. 2.

- **Circuit 1**. Comprising 3D rotation gates with all-to-all CNOT connections forming *strongly entangling layers*, this circuit demonstrates high entangling capacity and

low expressibility. It outperforms classical counterparts and some other PQC architectures, as shown in [22].

- **Circuit 2**. Constructed with a layer of Hadamard gates, followed by all-to-all CZ connections and an additional layer of rotations, this PQC boasts the highest entangling capacity among the circuits investigated in the study from Ref. [20].
- **Circuit 3**. Composed by Y-axis rotations followed by a layer of CNOT gates, this PQC exhibits high entangling capacity and low expressibility. Frequently categorized with *basic entangling layers*, it incorporates fewer training parameters than Circuit 1.
- **Circuit 4**. Featuring two layers of Y-axis rotations and two layers of controlled X-axis rotations, this PQC achieves a significant balance between entangling capacity and expressibility. However, it entails higher complexity compared to Circuits 1-3.
- **Circuit 5**. Similar to Circuit 4, but incorporating Z-axis rotations instead of X-axis rotations.
- **Circuit 6**. Comprising two layers of both X-axis and Z-axis rotations, along with two layers of all-to-all controlled rotations around the X-axis, this circuit was the most expressive circuit in the study from Ref. [20]. Nevertheless, it also presents the highest complexity among the considered circuits.

### II-B. Training Dataset

The PDBbind dataset [23] (2020 version) is adopted as the input to train the proposed quantum fusion model. PDBbind represents an extensive compilation of experimentally determined binding affinity data between proteins and ligands. This dataset meticulously associates protein-ligand complexes with their respective affinity measurements, a curation process executed via manual extraction from peer-reviewed scientific publications. The latest PDBbind version, released in early 2020, contains a total of 19,443 protein-ligand complexes. Additionally, a meticulously curated subset of 5,316 samples has been compiled, specifically comprising high-quality complexes. Finally, an even higher-quality core set of 285 samples is derived, primarily for validating binding affinity prediction methods. We utilize the refined set in the training and validation phases of our analysis, with 25% of the data reserved for validation. Then, the core set is used for the testing phase.

### II-C. Data Pre-processing

Before passing the PDBbind data into the two CNN architectures, it is essential to pre-process the raw data and extract pertinent input features from the 3D structures of proteins and ligands. In this regard, our approach closely aligns with established featurization techniques as outlined in [11], [13], [24], thereby facilitating the comparability of our results with existing state-of-the-art models. Moreover, the PDB files are converted to Mol2 files using the UCSF Chimera sofware [25].

The input data for 3D-CNN consists of spatial representation of 3D structures of atoms of protein-ligand pairs. The atoms are voxelized into a grid of size $N \times N \times N$ with a voxel size of 1 Å, and the number of voxels set to $N = 48$ to strike a balance between covering the entire pocket regions and lowering the input data size for the CNN model. $C = 19$ features are extracted for each voxelized atom using OpenBabel [26], bringing the input data for 3D-CNN to a $C \times N \times N \times N$ matrix. Such features include the atom type, hybridization, number of heavy atom bonds, number of bonds with heteroatoms, structural properties, partial charge, and molecule type (protein vs ligand). On the other hand, the input data for SG-CNN consists of a spatial graph representation of the protein-ligand complexes, with the atoms forming the nodes, and the bonds between atoms forming the edges, of the graph. As in Ref. [11], covalent bonds are represented by an $N \times N$ adjacency matrix and non-convalent bonds by an $N \times M$ matrix, where the element $A_{ij}$ of each matrix represents the Euclidean distance between the atoms $i$ and $j$.

## III. PROPOSED QUANTUM ERROR MITIGATION SCHEME

One of the primary hurdles faced by today's NISQ devices is the inherent presence of noise, resulting in the execution of quantum operations with limited coherence time. This noise adversely impacts the accuracy of quantum algorithms. In this section, we describe the different quantum noise channels, and introduce our proposed quantum error mitigation algorithm which is then customized to our quantum fusion model. In fact, although the quantum fusion model employed in this work is trained through quantum simulations, we have systematically assessed its performance under varying noise conditions using three distinct noise models. The first noise model is represented by the *amplitude damping channel*, with a probability parameter $p$, capturing energy dissipation from a quantum state to its environment. The second noise model is represented by the *phase damping channel*, with a probability parameter $p$, replicating the loss of quantum information without an accompanying loss of energy. The last error model is represented by the *depolarizing channel*, where a Pauli ($X$, $Y$, or $Z$) error occurs with equal probability $p$. A detailed analysis of the different noise sources and models is out of this paper's scope. See [27] for more details.

To alleviate the noise present in the post-execution outputs of the quantum algorithm, our ML-based quantum error mitigation algorithm is introduced. In particular, our quantum error mitigation scheme involves training an ML model specifically tailored to correct errors stemming from noisy quantum circuits. This method, called *data regression error mitigation* (DRER), is an extension of a prior work [13]

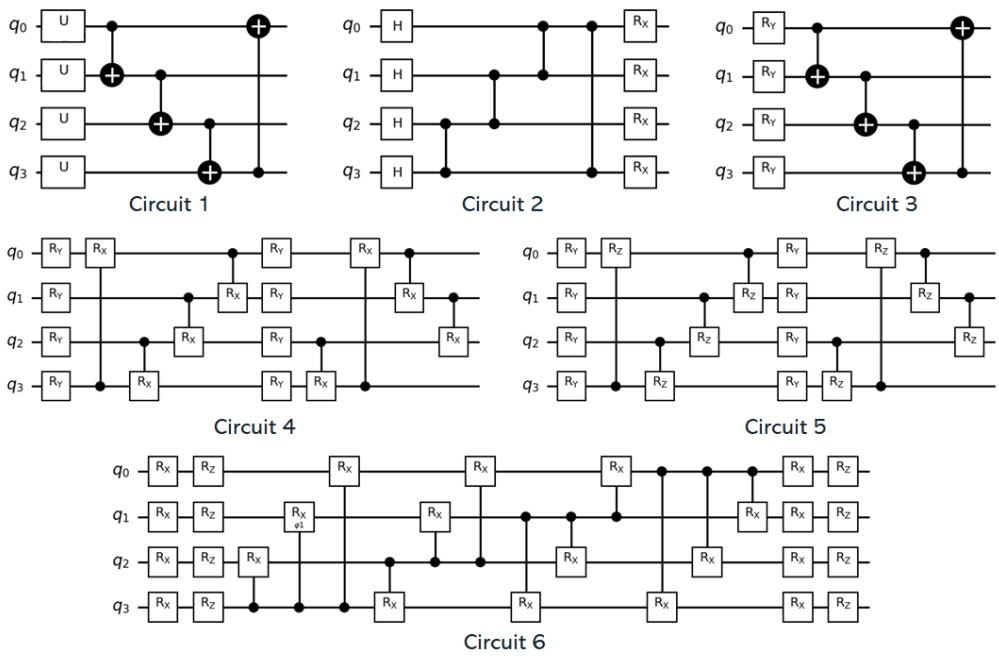


**Fig. 2**. Parametrized quantum circuits used as the ansatz of the quantum fusion model, labeled by their ID. Each figure represents a single layer of the final circuit, which can be repeated.

and has been customized specifically for our quantum fusion model. A schematic representation of our error mitigation algorithm is illustrated in Fig. 3. The resulting mitigated quantum fusion model incorporates an additional DREM classical layer designed to mitigate errors stemming from the noisy QNN. This classical layer comprises two fully-connected layers, with dimensions 32 and 16, respectively. Prior to training the quantum fusion model, the DRER layer undergoes training to learn to perform error mitigation by processing examples of both noisy and noiseless outputs. The layer's parameters are fine-tuned by minimizing the mean squared error with $\mathcal{L}^2$ regularization between the noisy and noiseless outputs:

$$\text{MSE}_R = \frac{1}{N_s}\sum_{i=0}^{N_s}[\hat{y}_i - y_i]^2 + \alpha||W||^2, \qquad (1)$$

where $N_s$ is the number of samples in the training set, $\hat{y}_i$ is the $i$-th prediction of the DREM layer, $\alpha$ is the regularization parameter, and $||\cdot||$ is the $L^2$ norm. Once trained, the DRER layer is integrated into the mitigated quantum fusion model, as illustrated in Fig. 3. Subsequently, the DREM layer remains unaltered during the fusion model's training and operates solely as a corrective element for the noisy outputs of the model. Consequently, once the DREM layer is trained, it can be employed multiple times with no quantum overhead and minimal (classical) computational expense.

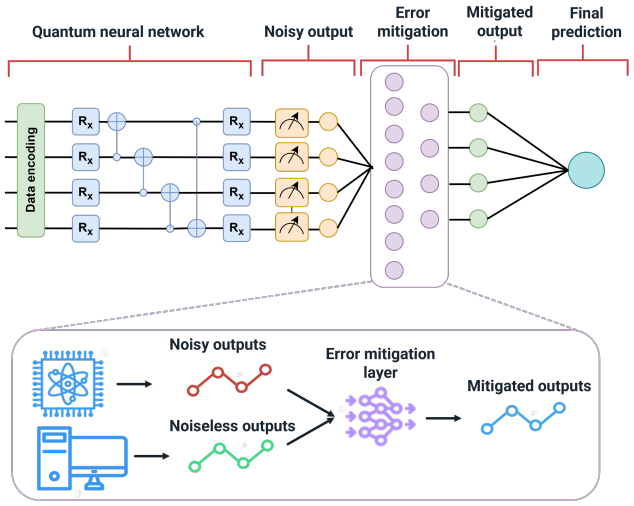


**Fig. 3**. Architecture of the proposed DREM algorithm. The mitigated quantum fusion model uses an additional layer which performs error mitigation on the outputs of the noisy QNN.

## IV. EXPERIMENTS AND RESULTS

This section showcases conducted experiments, simulations, and result analysis. We validate our hybrid quantum fusion model by comparing it with a classical fusion counterpart. The binding affinity prediction performance of both fusion models is evaluated using five different metrics: root mean square error (RMSE), mean absolute error (MAE), $R^2$, Pearson coefficient, and Spearman coefficient. Optimal performance entails minimizing RMSE and MAE while maximizing $R^2$, Pearson, and Spearman coefficients.

**Table I**. Comparison of classical and quantum fusion models.

| Method | $R^2$ | MAE | Pearson | Spearman | RMSE |
|---|---|---|---|---|---|
| Class. Fsn | 0.60 | 1.05 | 0.777 | 0.766 | 1.37 |
| Q'tum Fsn | 0.63 | 1.04 | 0.809 | 0.815 | 1.29 |

**Table II**. Comparison of the quantum fusion models with different parametrized quantum circuits.

| ID | $R^2$ | MAE | Pearson | Spearman | RMSE | Time | #params |
|---|---|---|---|---|---|---|---|
| 1 | 0.63 | 1.04 | 0.809 | 0.815 | 1.29 | 5h 18min | 125 |
| 2 | 0.546 | 1.085 | 0.763 | 0.781 | 1.462 | 3h 36min | 45 |
| 3 | 0.508 | 1.104 | 0.728 | 0.738 | 1.523 | 3h | 45 |
| 4 | 0.536 | 1.099 | 0.765 | 0.772 | 1.479 | 7h 32min | 165 |
| 5 | 0.539 | 1.101 | 0.774 | 0.779 | 1.473 | 7h 10min | 165 |
| 6 | 0.344 | 1.186 | 0.599 | 0.603 | 1.758 | 12h 35min | 285 |

### IV-A. Experimental Setup

Following a comparative evaluation of various optimizers and hyperparameters, the training of both the classical and our proposed quantum fusion models is conducted using the ADAM optimizer with a learning rate of $\eta = 0.002$, a batch size of 100 samples, and a mean squared error loss function. Moreover, in the QNN, $\sigma_z$ Pauli operator projection measurements are performed on all qubits to extract the classical measurement outcomes. The final prediction is made with a classical linear layer with a ReLu activation function. The optimal number of layers of the PQC is studied while considering varying depths of $L \in [1, 14]$. In the proposed quantum error mitigation algorithm, the regularization parameter, $\alpha$, is set to $1 \times 10^{-5}$ in our simulations.

### IV-B. Binding affinity prediction performance

First, we compare the performance of the best quantum fusion model and its classical counterpart for the five considered metrics, which is summarized in Table I. From Table I, we notice that the quantum fusion model provides better performance for all five metrics, which represents an up to 6% improvement over the classical model.

### IV-C. Convergence of the quantum fusion model

Next, in Fig. 4, we compare the convergence of the loss function in the validation set for the quantum and classical fusion models. We notice from Fig. 4 that the convergence of the loss function for the quantum model is much smoother and stable than that of the classical model. Therefore, the quantum fusion model provides much more reliable predictions, which are less likely to produce overfitting in the training set.

### IV-D. Impact of the quantum architecture

The inset in Fig. 4 depicts the convergence patterns of these six circuit architectures. While the loss function remains smooth and stable compared to the classical model, Circuit 1, in particular, exhibits a lower convergence value in the validation set. Table II provides an overview of the performance of the six quantum fusion models, with $L = 10$ layers, revealing Circuit 1 as the clear frontrunner. Although the quantum fusion models of Circuits 2 and 3 demonstrate faster training with only 45 training parameters, their lower complexity proves insufficient for accurate exploration of the solution space. On the contrary, Circuit 4-6 exhibit excessive complexity for the limited training set. Therefore, Circuit 1 stands out as an optimal blend of complexity, expressibility, and entangling capacity.

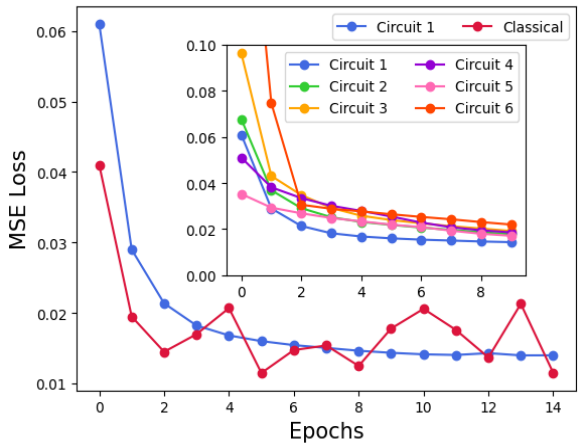


**Fig. 4**. Loss function convergence for the classical and best quantum fusion models, together with the convergence of the six parameterized quantum circuits with 10 layers.

Beyond the PQC design considerations, we conducted a comparative analysis of the quantum fusion model's performance using amplitude encoding and HAE techniques, as illustrated in Fig. 5. In this context, Circuit 1 with $L = 10$ serves as the chosen PQC. For HAE, parameters $b = 2$ and $m = 4$ were employed, corresponding to the encoding of 30 data points. The QNN input vector's 16 features were padded with zeros to create a 30-dimensional vector. The results depicted in Fig. 5 clearly demonstrate the superior performance of amplitude encoding over the HAE technique.

Furthermore, we explored the impact of the number of layers on the model's performance. Circuits with fewer layers exhibited higher errors due to limited access to the Hilbert space, while circuits with an abundance of layers increased the risk of overfitting to the training data, resulting in poorer generalization errors. Our analysis identified the optimal balance at $L = 10$ layers.

### IV-E. Quantum error mitigation

Figure 6 illustrates sample predictions from the quantum fusion models under various noise models and error probabilities. In particular, we consider three different noise probabilities, $p = 0.1, 0.05, 0.01$, which correspond to high, moderate, and low noise, respectively. Notably, all three noise models contribute to a reduction in the variability of binding affinity predictions. Specifically, at $p = 0.1$ and under depolarizing or amplitude damping noise, the noisy quantum fusion model predicts a constant value for binding

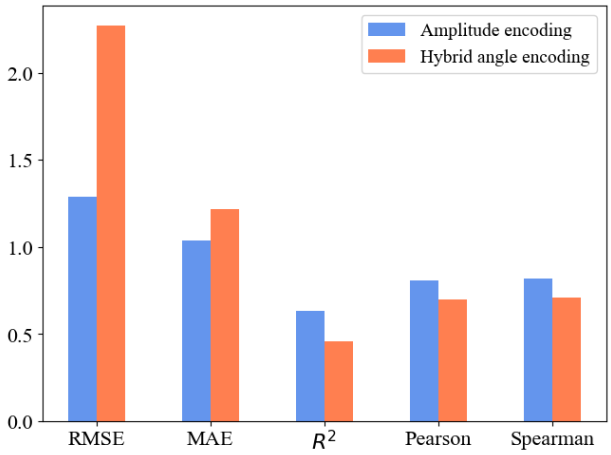


**Fig. 5**. Test statistics resulting from two data encoding schemes and strongly entangling layers with $L = 10$.

affinity. The primary distinction among the noise models lies in the phase damping channel, which exhibits a slower reduction in variability compared to the other two models.

For error rates $p \leq 0.05$, the DRER algorithm effectively mitigates the noisy outputs of the QNN. Despite the significant impact of noise on the quantum fusion model's predictions, the DRER algorithm successfully restores the original outputs, leading to a substantial improvement in binding affinity prediction accuracy. The comparative performance of noisy, mitigated, and noiseless models is depicted in Fig. 7.

Regarding the depolarizing channel, the DRER method consistently enhances all error metrics for all error probabilities, bringing them closer to noiseless results. The most substantial improvement is observed at $p = 0.05$, whereas at $p = 0.1$, a notable loss of information occurs, and at $p = 0.01$, the disparity between noisy and noiseless metrics is less pronounced.

Concerning the amplitude damping channel, the DRER method effectively corrects the quantum fusion model's output for error probabilities up to $p = 0.05$, while at $p = 0.1$, information loss impedes DREM's ability to mitigate outputs. The most significant performance gap occurs at $p = 0.05$, with a diminished effect observed at $p = 0.01$ when noisy and noiseless metrics are more comparable.

Finally, for phase damping noise, the DRER method successfully corrects the quantum fusion model's output for all probabilities. At $p = 0.01$, the DRER method notably improves all error metrics, aligning them more closely with noiseless results. However, for other probability values, where noisy and noiseless metrics exhibit less disparity, the DREM method has a relatively marginal impact on the outcomes.

The DREM approach has been compared to the standard Zero Noise Extrapolation (ZNE) [28] (with global folding and a scale factor of 3) for the depolarizing noise with $p = 0.05$. As can be seen in Fig. 7, the ZNE provides suboptimal results compared to the DREM. Moreover, the resulting ZNE model incurred a $3\times$ overhead in number of quantum gates, leading to a $10\times$ increase in training times. In contrast, our method introduced overhead only during the training of the DREM layer, representing a mere 10% of the overall model training time. While the experiments presented in this work are based on quantum simulations, future works will include further investigations of the proposed model's performance on actual quantum devices.

## V. CONCLUSION

In this paper, we have proposed a novel hybrid QML model, offering accurate and reliable binding affinity predictions, which is a critical factor in drug discovery. The proposed model is a quantum fusion model that integrates 3D-CNN and SG-CNN classical models with QNNs. A thorough exploration of the circuit architecture and design has been performed, providing an optimal design of the quantum fusion model. Simulation results have validated the superiority of the quantum model relative to the classical fusion counterpart model, demonstrating a 6% accuracy enhancement while achieving faster and smoother convergence, thus mitigating the risk of overfitting. Moreover, we have proposed an ML-based quantum error mitigation algorithm that outperforms existing error mitigation techniques. The proposed DREM algorithm provides optimal error mitigation for error probabilities $p \leq 0.05$ without incurring additional overhead.

### CODE AVAILABILITY

The code used in this work can be found at Ingenii's open access library: https://github.com/ingenii-solutions/ingenii-quantum-hybrid-networks/. The data used for this study is publicly available at http://www.pdbbind.org.cn/ [29].

## VI. REFERENCES

[1] M. D. Parenti and G. Rastelli, "Advances and applications of binding affinity prediction methods in drug discovery," *Biotechnology advances*, vol. 30, no. 1, pp. 244–250, 2012.

[2] G. Liu, D. Catacutan, K. Rathod, and et al., "Deep learning-guided discovery of an antibiotic targeting *Acinetobacter baumannii*," *Nat. Chem. Biol.*, 2023.

[3] V. Govind Kumar, A. Polasa, S. Agrawal, T. K. S. Kumar, and M. Moradi, "Binding affinity estimation from restrained umbrella sampling simulations," *Nature Computational Science*, vol. 3, no. 1, pp. 59–70, 2023.

[4] J. Paggi, J. Belk, S. Hollinsworth, and et al., "Leveraging nonstructural data to predict structures and affinities of protein-ligan complexes," *Proc. Nat. Acad. Sci.*, vol. 118, p. e2112621118, 2021.

[5] K. H. Bleicher, H.-J. Böhm, K. Müller, and A. I. Alanine, "Hit and lead generation: beyond high-throughput screening," *Nature reviews Drug discovery*, vol. 2, no. 5, pp. 369–378, 2003.

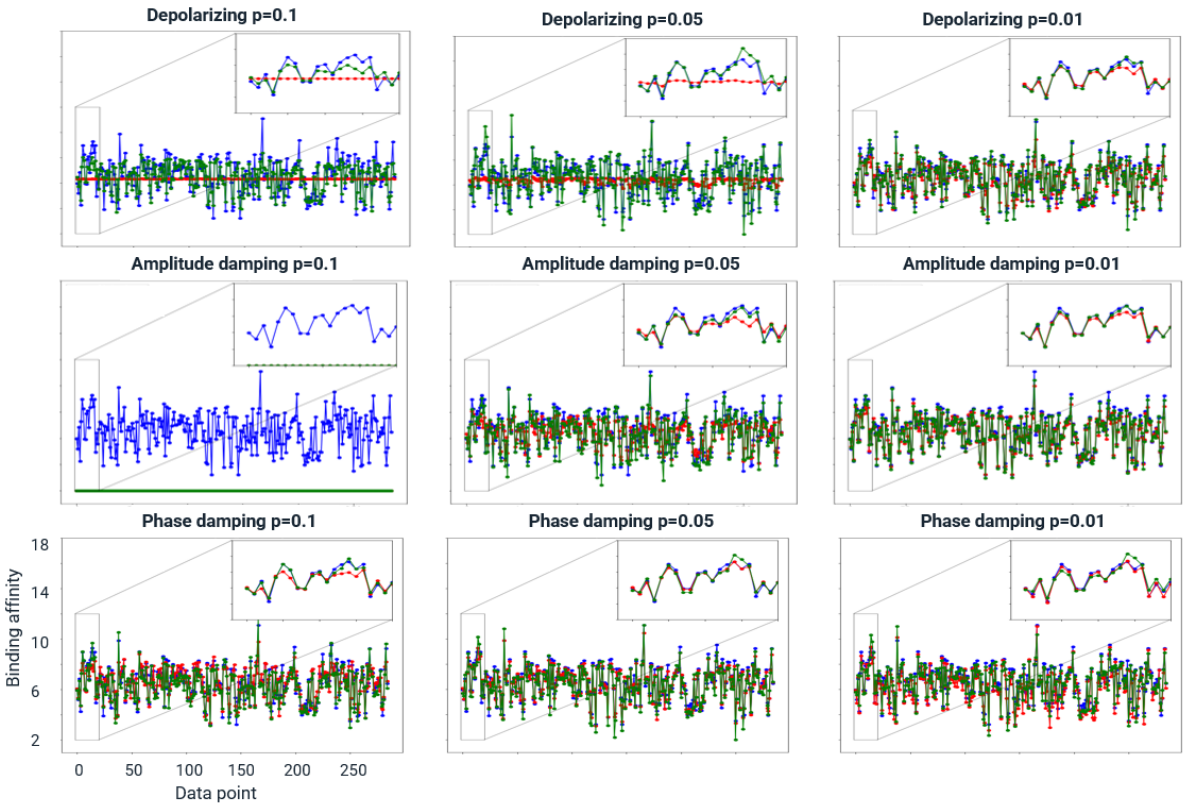


**Fig. 6**. Prediction of the quantum fusion model for the three noise models and different error probabilities. Noiseless predictions are represented by blue curves, noisy predictions by red curves, and mitigated predictions by green curves. For easier visualization, only the first 300 data samples are displayed in the figure.


[6] J. Vamathevan, D. Clark, P. Czodrowski, I. Dunham, E. Ferran, G. Lee, B. Li, A. Madabhushi, P. Shah, M. Spitzer *et al.*, "Applications of machine learning in drug discovery and development," *Nature reviews Drug discovery*, vol. 18, no. 6, pp. 463–477, 2019.

[7] Y. Cao, J. Romero, and A. Aspuru-Guzik, "Potential of quantum computing for drug discovery," *IBM Journal of Research and Development*, vol. 62, no. 6, pp. 6–1, 2018.

[8] K. Batra, K. M. Zorn, D. H. Foil, E. Minerali, V. O. Gawriljuk, T. R. Lane, and S. Ekins, "Quantum machine learning algorithms for drug discovery applications," *Journal of chemical information and modeling*, vol. 61, no. 6, pp. 2641–2647, 2021.

[9] J. Jiménez, M. Skalic, G. Martinez-Rosell, and G. De Fabritiis, "K deep: protein–ligand absolute binding affinity prediction via 3d-convolutional neural networks," *Journal of chemical information and modeling*, vol. 58, no. 2, pp. 287–296, 2018.

[10] Y. Kwon, W.-H. Shin, J. Ko, and J. Lee, "Ak-score: accurate protein-ligand binding affinity prediction using an ensemble of 3d-convolutional neural networks," *International journal of molecular sciences*, vol. 21, no. 22, p. 8424, 2020.

[11] D. Jones, H. Kim, X. Zhang, A. Zemla, G. Stevenson, W. F. D. Bennett, D. Kirshner, S. E. Wong, F. C. Lightstone, and J. E. Allen, "Improved protein–ligand binding affinity prediction with structure-based deep fusion inference," *Journal of Chemical Information and Modeling*, vol. 61, no. 4, pp. 1583–1592, 2021.

[12] S. Mensa, E. Sahin, F. Tacchino, P. Kl Barkoutsos, and I. Tavernelli, "Quantum machine learning framework for virtual screening in drug discovery: a prospective quantum advantage," *Machine Learning: Science and Technology*, vol. 4, no. 1, p. 015023, 2023.

[13] L. Domingo, M. Djukic, C. Johnson, and F. Borondo, "Hybrid quantum-classical convolutional neural networks to improve molecular protein binding affinity predictions," *arXiv preprint arXiv:2301.06331*, 2023.

[14] K. He, X. Zhang, S. Ren, and J. Sun, "Deep residual learning for image recognition," in *Proceedings of the IEEE conference on computer vision and pattern recognition*, 2016, pp. 770–778.

[15] T. Hur, L. Kim, and D. K. Park, "Quantum convolutional neural network for classical data classification," *Quantum Machine Intelligence*, vol. 4, no. 1, p. 3, 2022.

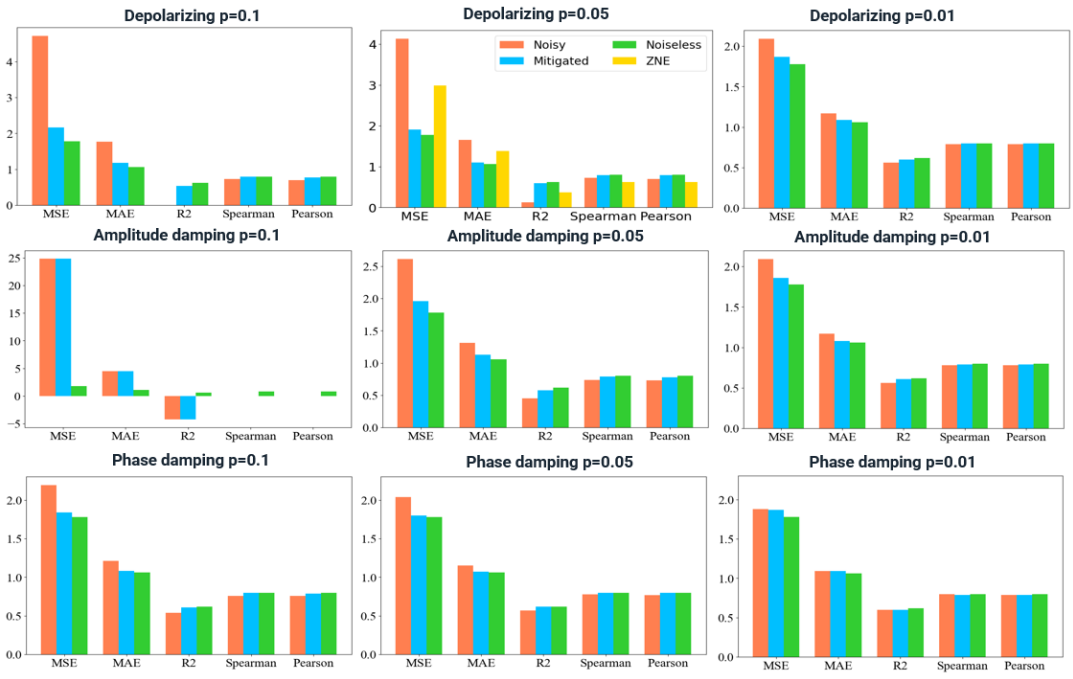


**Fig. 7**. Performance of the DREM and ZNE algorithms evaluated using the five error metrics considered in this work, for different noise models and error rates.


[16] J. Qi, C.-H. H. Yang, P.-Y. Chen*, and M.-H. Hsieh*, "Theoretical error performance analysis for variational quantum circuit based functional regression," *npj Quantum Information*, vol. 9, no. 4, 2023.

[17] I. F. Araujo, D. K. Park, F. Petruccione, and A. J. da Silva, "A divide-and-conquer algorithm for quantum state preparation," *Scientific reports*, vol. 11, no. 1, p. 6329, March 2021.

[18] C.-H. H. Yang, J. Qi, Y.-C. Chen, Y. Tsao, and P.-Y. Chen, "When BERT meets quantum temporal convolutional learning for text classification in heterogeneous computing," in *IEEE Intl. Conf. Acoustic, Speech, and Signal Processing*, 2022.

[19] J. Qi and J. Tejedor, "Classical-to-quantum transfer learning for spoken command recognition based on quantum neural networks," in *IEEE Intl. Conf. on Acoustics, Speech, and Signal Processing*, 2022.

[20] S. Sim, P. D. Johnson, and A. Aspuru-Guzik, "Expressibility and entangling capability of parameterized quantum circuits for hybrid quantum-classical algorithms," *Advanced Quantum Technologies*, vol. 2, no. 12, p. 1900070, 2019.

[21] D. A. Meyer and N. R. Wallach, "Global entanglement in multiparticle systems," *Journal of Mathematical Physics*, vol. 43, no. 9, pp. 4273–4278, 2002.

[22] C. Tüysüz, C. Rieger, K. Novotny, and et al., "Hybrid quantum classical graph neural networks for particle track reconstruction," *Quantum Machine Intelligence*, vol. 3, p. 29, 2021.

[23] wwPDB consortium, "Protein Data Bank: the single global archive for 3D macromolecular structure data," *Nucleic Acids Research*, vol. 47, no. D1, pp. D520–D528, 2018.

[24] M. M. Stepniewska-Dziubinska, P. Zielenkiewicz, and P. Siedlecki, "Development and evaluation of a deep learning model for protein–ligand binding affinity prediction," *Bioinformatics*, vol. 34, no. 21, pp. 3666–3674, 05 2018.

[25] E. F. Pettersen, T. D. Goddard, C. C. Huang, G. S. Couch, D. M. Greenblatt, E. C. Meng, and T. E. Ferrin, "Ucsf chimera-a visualization system for exploratory research and analysis," *Journal of Computational Chemistry*, vol. 25, no. 13, pp. 1605–1612, 2004.

[26] T. Vandermeersch and G. Hutchison, "Open babel: An open chemical toolbox," *Journal of Chemoinformatics*, vol. 3, no. 33, 2011.

[27] M. A. Nielsen and I. L. Chuang, *Quantum Computation and Quantum Information: 10th Anniversary Edition*. Cambridge University Press, 2010.

[28] Y. Li and S. C. Benjamin, "Efficient variational quantum simulator incorporating active error minimization," *Phys. Rev. X*, vol. 7, p. 021050, 2017. [Online]. Available: https://link.aps.org/doi/10.1103/PhysRevX.7.021050

[29] wwPDB consortium, "Protein Data Bank: the single global archive for 3D macromolecular structure

data," *Nucleic Acids Research*, vol. 47, no. D1, pp. D520–D528, 10 2018. [Online]. Available: https://doi.org/10.1093/nar/gky949